

Kinematic characteristics of the Milky Way globular clusters based on *Gaia* DR2 data

I. V. Chemerynska^{1,7*}, M. V. Ishchenko^{2,3}, M. O. Sobolenko², S. A. Khoperskov^{4,5}, P. P. Berczik^{7,4,8,3}

¹Taras Shevchenko National University of Kyiv, Glushkova ave., 4, 03127, Kyiv, Ukraine

²Main Astronomical Observatory, National Academy of Sciences of Ukraine,
27 Akademika Zabolotnoho St., 03143, Kyiv, Ukraine

³Fesenkov Astrophysical Institute, Observatory 23, 050020 Almaty, Kazakhstan

⁴Leibniz-Institut für Astrophysik Potsdam (AIP), An der Sternwarte 16, 14482 Potsdam, Germany

⁵GEPI, Observatoire de Paris, Université PSL, CNRS, 5 Place Jules Janssen, 92190 Meudon, France

⁶National Astronomical Observatories and Key Laboratory of Computational Astrophysics, Chinese Academy of Sciences,
20A Datun Rd., Chaoyang District, 100101 Beijing, China

⁷Institut d'Astrophysique de Paris, CNRS - Sorbonne Université, 98bis boulevard Arago, 75014 Paris, France

⁸Konkoly Observatory, Research Centre for Astronomy and Earth Sciences, Eötvös Loránd Research Network (ELKH), MTA
Centre of Excellence, Konkoly Thege Miklós út 15-17, 1121 Budapest, Hungary

Using the data from *Gaia* (ESA) Data Release 2 we performed the orbital calculations of globular clusters (GCs) of the Milky Way. To explore possible close encounters (or collisions) between the GCs, using our own developed high-order φ -GRAPE code, we integrated backward and forward orbits of 119 objects with reliable positions and proper motions. In calculations, we adopted a realistic axisymmetric Galactic potential (*bulge + disk + halo*). Using different impact conditions, we found four pairs of the six GCs that may have experienced an encounter within twice the sum of the half-mass radii (“collisions”) over the last 5 Gyr: Terzan 3 – NGC 6553, Terzan 3 – NGC 6218, Liller 1 – NGC 6522 and Djorg 2 – NGC 6553.

Key words: Galaxy: globular clusters: general - Galaxy: kinematics and dynamics - methods: numerical

INTRODUCTION

It is believed that GCs in the Milky Way (MW) are old gravitationally bound systems of stars with typical ages $\gtrsim 6$ Gyr and masses $\gtrsim 10^4 M_\odot$ [13]. These objects are a powerful tool to examine the Galactic structure and assembly history at different scales from the star clusters formation to hierarchical merger events [14]. The recent precise astrometric measurements from *Gaia* Data Release 2 (DR2) [8] provide a possibility to measure the mean proper motions for ≈ 150 GCs in the MW which makes it possible to study the orbital evolution of the GCs system as the whole.

In this work, we aim to explore the close encounters between different GCs and find the pairs of the GCs which have an encounter within twice the sum of the half-mass radii (“collisions”). In order to do that, using two GCs catalogs [5, 23], we study the dynamics of the GCs as the test-particles in the axisymmetric MW-like potential over the last 5 Gyr [1, 2, 10, 17, 19–21].

GLOBULAR CLUSTER SAMPLE

Prior to the orbital integration, we prepared a complete catalog of the GCs. For this purpose, we combined two recent catalogs [5, 23] which contain information on 152 objects (see Table 3). The resulting catalog contains the complete phase-space information required to set the initial conditions in our simulations: right ascension (RA), declination (DEC) and distance (D), proper motions $\mu_{\alpha*} = \mu_\alpha \cos \delta$, μ_δ and radial velocity v_r .

To avoid the calculation of the GCs orbits with large uncertainties of initial conditions we first performed an analysis of the errors of the *Gaia* measurement required for our simulations. In Fig. 1 we show the relative errors for the radial velocity and proper motions where each GC has its own index (see Table 3). The obtained uncertainties for the radial velocity (v_r) lie in the range of [-10%, +15%] for all studied GCs. The analysis of the uncertainties for proper motions ($\mu_{\alpha*}$, μ_δ) showed that its value

*chemerynskaira@gmail.com

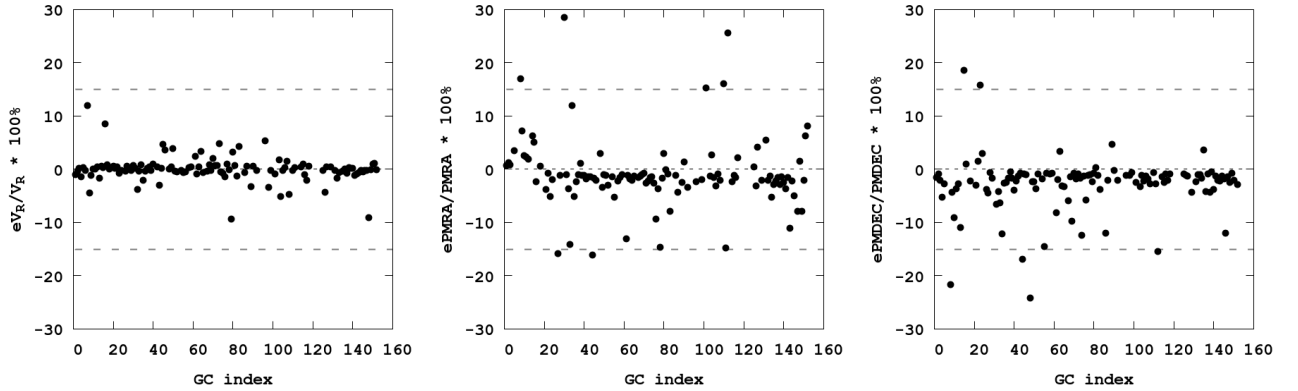


Fig. 1: Distribution of the GCs measurement errors for radial velocity v_r (left) and proper motions in right ascension (μ_{α^*} , center) and in declination (μ_{δ} , right). Dashed gray horizontal lines indicate 15% confidence range.

can exceeds 30% for some individual GCs in our sample. Therefore, the GCs with the relative error larger than 30% for radial velocity and proper motions were removed from our catalogue and further analysis. See 8 GCs marked as *me* (measurement error) in Table 3.

For calculating positions and velocities in the Galactocentric rest-frame (for basic coordinate transformation see [12]), we accepted an in-plane distance of the Sun from the Galactic center and the plane as $X_{\odot} = 8.178$ kpc [9] and $Z_{\odot} = 20.8$ pc [6], a velocity of the Local Standard of Rest (LSR), $V_{\text{LSR}} = 234.737$ [15], and a peculiar velocity of the Sun with respect to the LSR, $U_{\odot} = 11.1$ km s $^{-1}$, $V_{\odot} = 12.24$ km s $^{-1}$, $W_{\odot} = 7.25$ km s $^{-1}$ [22].

We assume the initial positions and velocities of the GCs in the heliocentric coordinate system as (X, Y, Z) and (U, V, W) , respectively. As a result, the initial positions (x, y, z) and velocities (u, v, w) of the GCs in the rectangular galactic coordinates can be derived from the positions and velocities of the GCs in the heliocentric coordinate system (X, Y, Z) and (U, V, W) as follows:

$$\begin{cases} x = X + X_{\odot} + X_{\text{LSR}}, \\ y = Y + Y_{\odot} + Y_{\text{LSR}}, \\ z = Z + Z_{\odot} + Z_{\text{LSR}}, \end{cases} \quad (1)$$

$$\begin{cases} u = U + U_{\odot} + U_{\text{LSR}}, \\ v = V + V_{\odot} + V_{\text{LSR}}, \\ w = W + W_{\odot} + W_{\text{LSR}}, \end{cases} \quad (2)$$

where we adopt $U_{\text{LSR}} = W_{\text{LSR}} = 0$ and $Y_{\odot} = 0$.

ORBITS INTEGRATION

For the GCs orbit integration we adopted the MW-type gravitational potential based on the su-

perposition of *bulge + disk + halo* models. In particular, the total potential consisting of a spherical bulge $\Phi_b(R, z)$, an axisymmetric disk $\Phi_d(R, z)$ and a spherical dark-matter halo $\Phi_h(R, z)$ can be written as follows:

$$\Phi(R, z) = \Phi_b(R, z) + \Phi_d(R, z) + \Phi_h(R, z), \quad (3)$$

where $R^2 = x^2 + y^2$ is the Galactocentric distance in polar coordinates and z is the vertical coordinate perpendicular to the disk plane.

Potentials of the bulge and the disk were taken in the form of Miyamoto-Nagai [16], while the dark matter potential is in the form of Navarro-Frenk-White (NFW) profile [18]:

$$\begin{cases} \Phi_b(R, z) = -\frac{M_b}{(r^2 + b_b^2)^{1/2}}, & (4) \\ \Phi_d(R, z) = -\frac{M_d}{\left[R^2 + \left(a_d + \sqrt{z^2 + b_d^2} \right)^2 \right]^{1/2}}, & (5) \\ \Phi_h(R, z) = -\frac{M_h}{r} \ln \left(1 + \frac{r}{b_h} \right), & (6) \end{cases}$$

where $r = \sqrt{R^2 + z^2}$ is the spherical galactocentric distance, while masses and the scale-lengths of the components are shown in Table 1 [3, 4].

For the GCs orbital integration we used a high-order parallel dynamical N -body code φ -GRAPE which is based on the fourth-order Hermite integration scheme with hierarchical individual block time steps scheme [7]. More details about the code architecture and special GRAPE hardware can be found in [11].

Before moving forward in the analysis of the collisions of the GCs population we have tested our numerical setup in order to keep tracking the GCs whose orbits are the same during backward and forward integration. First, we integrated all 152 GCs

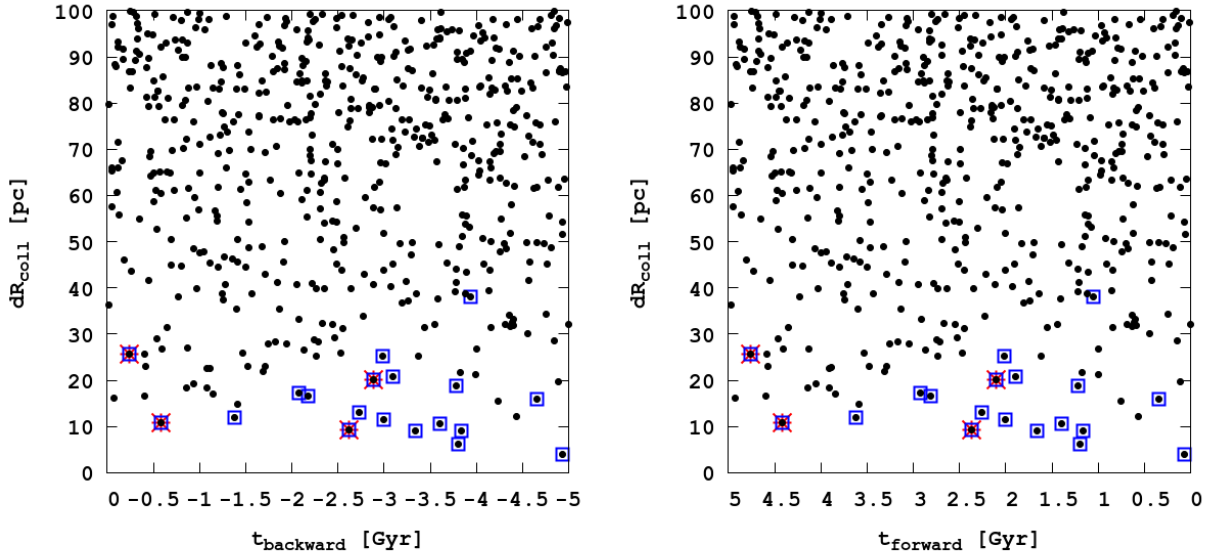


Fig. 2: Relative separation of the GC collision pairs (black dots) in backward (left) and forward (right) integration. Open squares indicate the collisions with $dR_{\text{coll}} < 2(R_{\text{hm},i} + R_{\text{hm},j})$ and asterisks indicate the collisions with $dV_{\text{coll}} < 200 \text{ km s}^{-1}$.

backward for 5 Gyr then we use the positions of velocities of all the GCs at the end of the simulations and integrate them forward for 5 Gyr. One could expect that the resulting positions and velocities should be identical to the observed ones. However, we have found that the orbits of 25 GCs are not invertible. These GCs usually pass very close to the galactic center and most likely even an adaptive time-step is not able to capture their motions in close proximity to the centre. Another possibility is a non-integrability of the potential (i.e. it is hard to quantify) and we leave this issue for further studies. These GCs as *to* (type of orbit) in Table 3 and they were removed from further analysis. As a result, our final sample consists of 119 objects.

Table 1: Galactic potential parameters.

Parameter	Value	Unit
Bulge mass M_b	1.03×10^{10}	M_\odot
Disk mass M_d	6.51×10^{10}	M_\odot
Halo mass M_h	29.00×10^{10}	M_\odot
Bulge scale param. b_b	0.2672	kpc
Disk scale param. a_d	4.4	kpc
Disk scale param. b_d	0.3084	kpc
Halo scale param. b_h	7.7	kpc

GC COLLISION PAIRS

In order to count the possible maximum number of collisions between all the pairs of GCs we first check all the close encounters during the simulation time with the maximum separation up to < 100 pc. Resulting in 2019 and 1973 close encounters in our sample during the backward and forward orbits integration, respectively.

We define a close encounters as “collisions” if (i) the minimum distance between the GCs is less than half the sum of their half-mass radii: $dR_{\text{coll}} < 2(R_{\text{hm},i} + R_{\text{hm},j})$ and (ii) also the relative velocity between these objects at the same time dV_{coll} is $< 200 \text{ km s}^{-1}$. The first collision condition (i) reduces numbers to only 18 events, while applying the second (ii) condition we obtained only four reliable collision events.

Fig. 2 shows the separation parameter as a function of time for backward (left) and forward (right) integration where four reliable collisions (Terzan 3 - NGC 6553, Terzan 3 - NGC 6218, Liller 1 - NGC 6522, Djorg 2 - NGC 6553) are marked by red symbols. It is worth mentioning, that all the colliding GCs were likely originally formed in the MW disk [14].

In order to estimate the global collision rate, in Fig. 3 we show the cumulative collisions number as a function of GCs minimum impact parameter dR_{coll} (left) and relative velocity dV_{coll} (right) at the moment of collision. According to this figure, we can estimate that these plots show that in each ten million

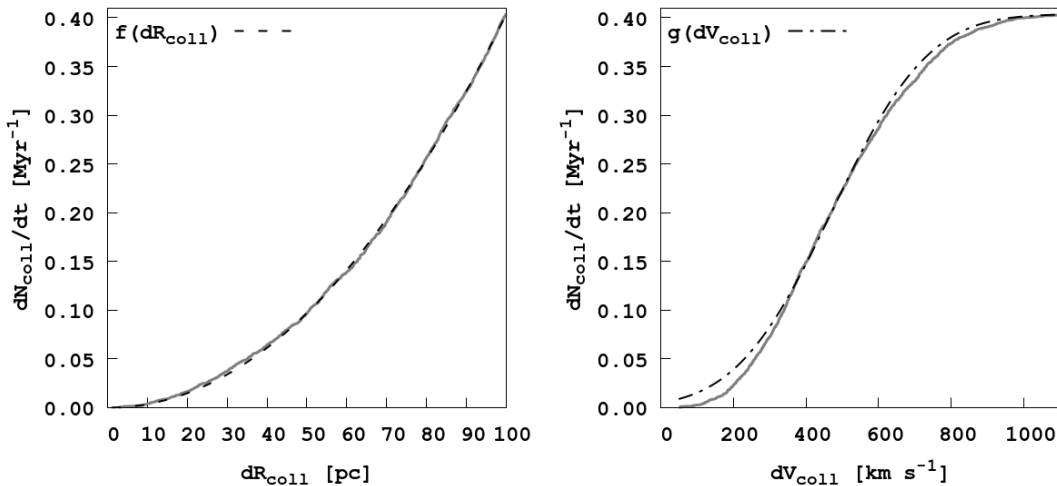


Fig. 3: GCs collision rate as a function of the relative distance distribution (left) and relative velocity (right). Black dashed line (left) is a power-law fit $f(x)$ for relative distance (see equation (7)) and dash-dotted line (right) is cumulative distribution function fit $g(x)$ for relative velocity (see equation (8)).

years there is at least one collision with the impact parameter less than 50 pc and less than 300 km s^{-1} .

From the cumulative collision number distributions we found the minimum value of impact parameter and relative velocity are $dR_{\text{coll}} \approx 5 \text{ pc}$ and $dV_{\text{coll}} \approx 85 \text{ km s}^{-1}$, respectively. The distribution with the impact parameter was fitted by a simple power-law function:

$$\frac{dN_{\text{coll}}}{dt}(dR_{\text{coll}}) = 10^{a \cdot \lg(dR_{\text{coll}}) + b}, \quad (7)$$

where the best fit slope parameters are $a = 2.06$ and $b = -4.51$. On the contrary, the velocity distribution was fitted by the cumulative normal distribution function:

$$\frac{dN_{\text{coll}}}{dt}(dV_{\text{coll}}) = \frac{1}{2} \left[1 + \text{erf} \left(\frac{dV_{\text{coll}} - \mu}{\sigma \sqrt{2}} \right) \right], \quad (8)$$

where we used as a best fit mean value $\mu = 472$ and the best fit variance value $\sigma = 209$.

In Fig. 4 we present the orbits of colliding GCs which are color-coded by time. The time range is about ten million years around the moment of collisions. More detailed the orbital structure is shown in right. The solid line corresponds to the first GC in a pair while the dashed line shows the second one. The intersection of the orbits (“collision”) is marked as a red circle. Note that our study presents the simplified scenario and more proper study of the GCs “collisions” of orbits requires considerations of the gravity interaction between the GCs.

In Table 2 we summarize the exact time of “collisions” together with the minimum separations and relative velocities at the exact moment of collision.

Table 2: Characteristics of GC collision pairs.

GC 1	GC 2	dR_{coll} (pc)	dV_{coll} (km s^{-1})	Time (Myr)	Prob. (%)
Terzan 3	NGC 6553	25.58	148.18	237	22.09
Terzan 3	NGC 6218	10.75	183.12	580	24.32
Liller 1	NGC 6522	9.38	185.04	2625	25.14
Djorg 2	NGC 6553	20.22	153.14	2889	20.23

To check the possible uncertainties introduced by the velocity errors (see Fig. 1) of *Gaia* measurements, we perform extra 10 thousand runs of backward integration with the $\pm \sigma$ randomly initialized and normally distributed velocities. The σ velocity errors (eV_R, ePMRA and ePMDEC) were taken from the [23] catalog. Following this way we can approximately estimate the probability that our four GSs to collide during the last 5 Gyr of evolution of our Galaxy. From this set of 10 thousand individual runs we obtained that our selected clusters “collide” in $\approx 11.21 \%$ of cases. Taking advantage of the randomization in the initial conditions, for each individual GCs pairs we also estimate the lower limit of the collisions probability (see the last column in Table 2).

CONCLUSIONS

Using the present-day *Gaia* DR2-based catalogs [5, 23] we have analyzed the orbits of the Milky Way globular clusters. From 152 GCs we discard 8 objects with large velocity errors and 25 GCs were removed from the analysis due to unstable orbits

during backward/forward integration. For the remaining 119 GCs, we analyze both backward and forward orbits calculated in the MW-like external potential using our own developed high order φ -GRAPE code. Using a complex criteria for the collisions detection we identified four candidate colliding pairs: Terzan 3 - NGC 6553, Terzan 3 - NGC 6218, Liller 1 - NGC 6522, Djorg 2 - NGC 6553. We also estimated the overall collision rate as about one collision with the impact parameter less than 50 pc and less than 300 km s^{-1} per 10 Myr. Our experimental overall close encounter (“collision”) number ($N_{\text{coll}}=4$) agrees well with the simple estimation from the collision rate statistical approximations (see Fig. 3).

ACKNOWLEDGEMENT

The authors thank the anonymous referee for a very constructive report and suggestions that helped significantly improve the quality of the manuscript. PB and MI acknowledge the support within grant № AP14869395 of the Science Committee of the Ministry of Science and Higher Education of Kazakhstan (“Triune model of Galactic center dynamical evolution on cosmological time scale”). The works of MI and MS were supported by the National Academy of Sciences of Ukraine under the research project of young scientists № 0121U111799. The work of PB, MI and MS was also supported by the Volkswagen Foundation under grant № 97778. The work of PB was also supported by the Volkswagen Foundation under a special stipend № 9B870. PB and MI acknowledge the support by the Ministry of Education and Science of Ukraine under the collaborative grant № M/32-23.05.2022.

This work has made use of data from the European Space Agency (ESA) mission GAIA (<https://www.cosmos.esa.int/gaia>), processed by the GAIA Data Processing and Analysis Consortium (DPAC, <https://www.cosmos.esa.int/web/gaia/dpac/consortium>). Funding for the DPAC has been provided by national institutions, in particular the

institutions participating in the GAIA Multilateral Agreement.

REFERENCES

- [1] Allen C., Moreno E., Pichardo B. 2006, *AJ*, 652, 2
- [2] Allen C., Moreno E., Pichardo B. 2008, *AJ*, 674, 1
- [3] Bajkova A.T., Bobylev V.V. *Astronomical and Astrophysical Transactions*, 2021, 32, 3, p. 177-206
- [4] Bajkova A.T., Bobylev V.V., 2021, *Research in Astronomy and Astrophysics*, 21, 173
- [5] Baumgardt H., Hilker M., Sollima A., Bellini A. 2019, *MNRAS*, 482, 4
- [6] Bennett M., Bovy J. 2019, *MNRAS*, 482, 1417
- [7] Berczik P., Nitadori K., Zhong S. et al. 2011, in *International conference on High Performance Computing*, Kyiv, Ukraine, p. 8-18
- [8] Gaia Collaboration: Helmi I., van Leeuwen F., McMillan P.J. et al. 2018, *A&A*, 616, A12
- [9] Gravity Collaboration: Abuter R., Amorim A., Bauböck M. et al. 2019, *A&A*, 625, L10
- [10] Gnedin O.Y., Ostriker J.P. 1997, *AJ*, 474, 1
- [11] Harfst S., Gualandris A., Merritt D. et al. 2007, *New Astron.*, 12, 357
- [12] Johnson D.R.H., Soderblom D.R. 1987, *AJ*, 93, 864
- [13] Kharchenko N.V., Piskunov A.E., Schilbach E., Röser S., Scholz R.D. 2013, *A&A*, 558, A53
- [14] Kruijssen J.M.D., Pfeffer J.L., Chevance M. et al. 2020, *MNRAS*, 498, 2
- [15] Mardini M.K., Placco V.M., Meiron Y. et al. 2020, *ApJ*, 903, 88
- [16] Miyamoto M., Nagai R. 1975, *Publications of the Astronomical Society of Japan*, 533-534, 27
- [17] Moreno E., Pichardo B., Velázquez H. 2014, *AJ*, 793, 2
- [18] Navarro J.F., Frenk C.S., White S.D.M. et al. 1997, *ApJ*, 490, 2
- [19] Pichardo B., Martos M., Moreno E. 2004, *AJ*, 609, 1
- [20] Pérez-Villegas A., Rossi L., Ortolani S. et al. 2018, *Publications of the Astronomical Society of Australia*, 35
- [21] Pérez-Villegas A., Barbuy B., Kerber L.O. et al. 2020, *MNRAS*, 491, 3
- [22] Schönrich R., Binney J., Dehnen W. 2010, *MNRAS*, 403, 4
- [23] Vasiliev E. 2019, *MNRAS*, 484, 2

Table 3: Initial list of GCs.

ID	Name	Flag	ID	Name	Flag	ID	Name	Flag	ID	Name	Flag	ID	Name	Flag
1	NGC 104		32	NGC 5634		63	NGC 6273		94	Terzan 5	to	125	NGC 6656	
2	NGC 288		33	NGC 5694		64	NGC 6284		95	NGC 6440	to	126	Pal 8	
3	NGC 362		34	IC 4499		65	NGC 6287		96	NGC 6441		127	NGC 6681	
4	Whiting 1		35	NGC 5824		66	NGC 6293	to	97	Terzan 6	to	128	NGC 6712	to
5	NGC 1261		36	Pal 5		67	NGC 6304		98	NGC 6453		129	NGC 6715	
6	Pal 1	me	37	NGC 5897		68	NGC 6316		99	NGC 6496		130	NGC 6717	to
7	E 1	me	38	NGC 5904		69	NGC 6341		100	Terzan 9	to	131	NGC 6723	
8	Eridanus		39	NGC 5927		70	NGC 6325		101	Djorg 2	cc	132	NGC 6749	
9	Pal 2		40	NGC 5946		71	NGC 6333		102	NGC 6517	to	133	NGC 6752	
10	NGC 1851		41	BH 176	me	72	NGC 6342		103	Terzan 10		134	NGC 6760	me
11	NGC 1904		42	NGC 5986		73	NGC 6356		104	NGC 6522	cc	135	NGC 6779	
12	NGC 2298		43	FSR 1716		74	NGC 6355		105	NGC 6535		136	Terzan 7	
13	NGC 2419		44	Pal 14		75	NGC 6352		106	NGC 6528		137	Pal 10	
14	Pyxis		45	BH 184		76	IC 1257		107	NGC 6539		138	Arp 2	
15	NGC 2808		46	NGC 6093		77	Terzan 2		108	NGC 6540		139	NGC 6809	
16	E 3		47	NGC 6121	to	78	NGC 6366		109	NGC 6544	to	140	Terzan 8	
17	Pal 3	me	48	NGC 6101		79	Terzan 4		110	NGC 6541		141	Pal 11	
18	NGC 3201		49	NGC 6144		80	BH 229		111	ESO 280-6		142	NGC 6838	
19	Pal 4	me	50	NGC 6139		81*	FSR 1758		112	NGC 6553	cc	143	NGC 6864	
20	Crater		51	Terzan 3	cc	82	NGC 6362		113	NGC 6558	to	144	NGC 6934	
21	NGC 4147		52	NGC 6171		83*	Liller 1	cc	114	Pal 7		145	NGC 6981	
22	NGC 4372		53	ESO 452-11	to	84	NGC 6380	to	115	Terzan 12		146	NGC 7006	
23	Rup 106		54	NGC 6205		85	Terzan 1	to	116	NGC 6569		147	NGC 7078	
24	NGC 4590		55	NGC 6229		86	Ton 2		117	BH 261		148	NGC 7089	
25	NGC 4833	to	56	NGC 6218	cc	87	NGC 6388		118	NGC 6584		149	NGC 7099	
26	NGC 5024		57	FSR 1735	me	88	NGC 6402	to	119	NGC 6624	to	150	Pal 12	
27	NGC 5053		58	NGC 6235		89	NGC 6401		120	NGC 6626	to	151	Pal 13	
28	NGC 5139		59	NGC 6254		90	NGC 6397		121	NGC 6638	to	152	NGC 7492	
29	NGC 5272		60	NGC 6256	to	91	Pal 6	to	122	NGC 6637	to			
30	NGC 5286	me	61	Pal 15		92	NGC 6426		123	NGC 6642	to			
31	NGC 5466		62	NGC 6266		93	Djorg 1	to	124	NGC 6652	to			

NOTE: Parameters for all GCs was taken from [23] with exception for GCs marked * with data from [5]. Column Flag contain additional information: me - GC was excluded from the integration due to their significant measurement errors, to - GC was excluded from the integration due to their type of orbit, cc - GC what satisfied "collision" conditions.

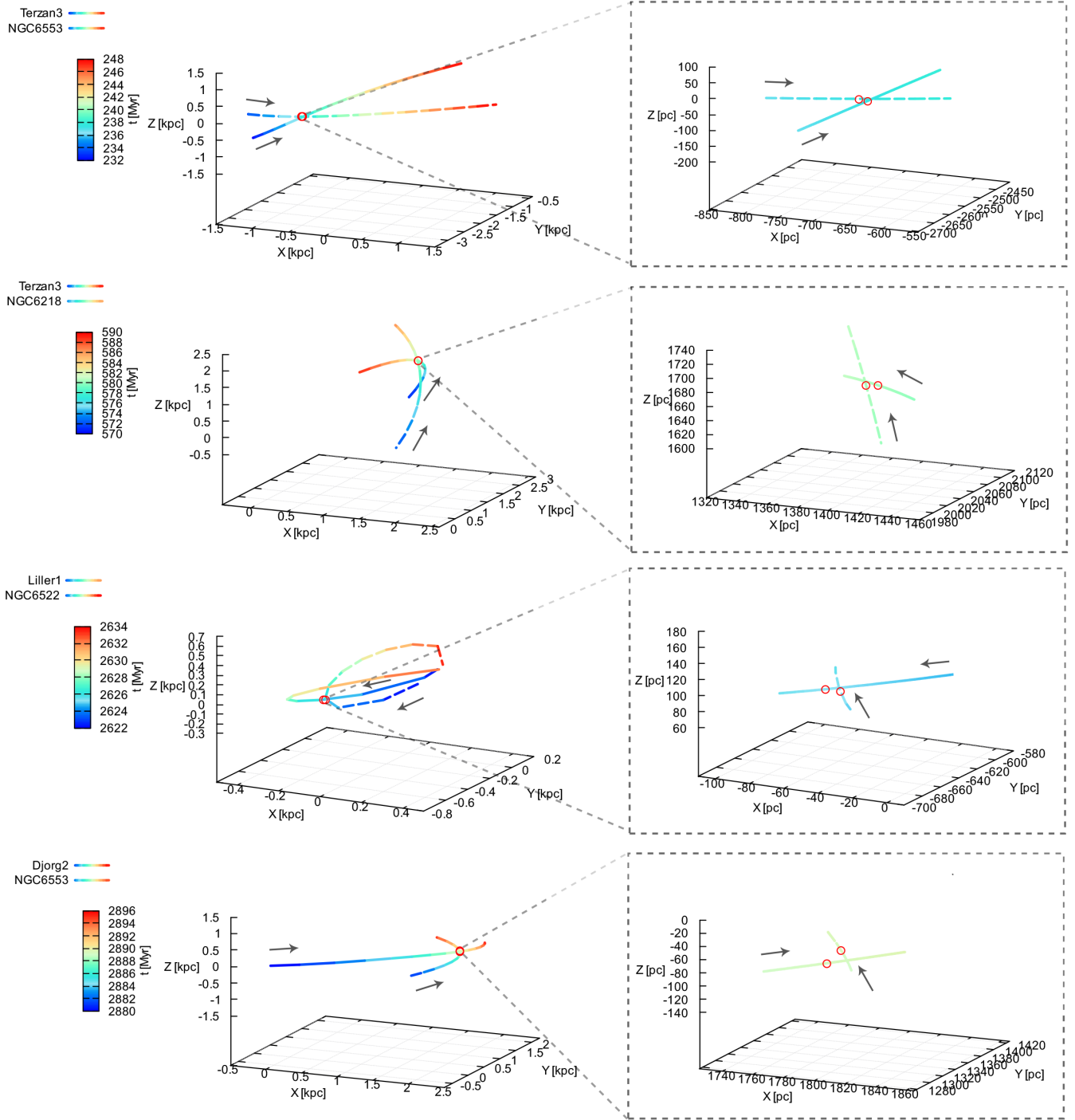


Fig. 4: 3D orbits of GC “collision” pairs in ~ 20 Myr (left) and ~ 1 Myr (right) around collision moment from (top) to (bottom): (Terzan 3, NGC 6553), (Terzan 3, NGC 6218), (Liller 1, NGC 6522) and (Djorg 2, NGC 6553). Trajectories are colour coded by time, where arrows indicate motion direction and open circles show time moment of collision.